Laser-Ultrasonics Wave Generation and Propagation FE Model in Metallic Materials

A. Cavuto[*,1], F. Sopranzetti[2], M. Martarelli[2], G.M. Revel[1]
[1]Università Politecnica delle Marche, Ancona, Italy
[2] Università e-Campus, Novedrate (CO), Italy
*Corresponding author: Department of Industrial Engineering and Mathematical Sciences, Università Politecnica delle Marche, via Brecce Bianche - Monte Dago - 60131 Ancona, Italy

Abstract: A 2D axisymmetric model was considered in order to evaluate the propagation paths of the ultrasonic waves generated inside an aluminum plate sample due to a rapid thermal expansion produced by laser pulse.
Laser Doppler Vibrometer is used to experimentally validate the numerical results of the wave propagation in the material.
The presented numerical model is able to identify directivity patterns for the longitudinal (P), transverse (T) and superficial (S) waves.
In Non-Destructive Testing (NDT) by Laser Ultrasonics, the development of models that identify the propagation paths of the ultrasonic waves is necessary to establish criteria that allow the defects identification especially in materials with complex shapes such as railway axles.

Keywords: laser ultrasonics, ultrasound, elastic waves, thermoelastic, lamb wave.

1. Introduction

The Laser Ultrasonics technique, based on generating ultrasonic waves as a result of laser pulse incident on material surface, is a valid Non-Destructive Testing (NDT) method for quality control and damage detection [1]. It has been successfully applied for diagnostics purpose to composite materials in the aeronautical field [2-4]. Complete models of the ultrasonic waves generation induced by the thermo-elastic stress produced by the impinging laser and their propagation would be of great interest in the design of experimental phase. In this paper an FE model of the ultrasonic wave generation and its propagation in metallic [5-8] has been investigated, which can be later applied to quality control of train axles.
Different physical processes may take place when a solid surface is irradiated by a laser: heating of a specific region, generation of thermal waves, generation of elastic wave (ultrasound) etc. Two phenomena can be the cause of ultrasound generation depending on the source laser energy density [9]: the thermoelasticity, i.e. the material thermal expansion, and the ablation, i.e. the plasma formation due to the abrupt heating with consequent material expulsion, see Figure 1. In the model described in this paper the laser power regimes which generate the thermo-elastic stress and strain will be considered.

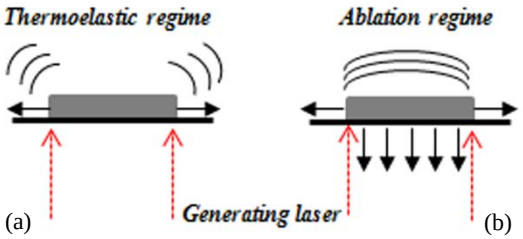

Figure 1. Laser generation of ultrasound in (a) thermoelastic regime and (b) ablative regime.

2. Governing Equations

The generation and propagation of elastic waves in a isotropic metallic material is an issue that involves both heat transfer in the solid and thermo-acoustics interaction mechanisms. For a semi-infinite, isotropic metal occupying the space $z \geq 0$, with a laser beam incident normally on the free surface $z = 0$, temperature and displacement in the metal in the thermoelastic regime can be described by the thermal diffusion equation and thermoelastic displacement equation [10]:

$$\rho C_v \frac{\partial T}{\partial t} + \rho C_v \boldsymbol{u}_1 \nabla T = \nabla(k\nabla T) + Q \tag{1}$$

$$(\lambda + \mu)\nabla(\nabla \boldsymbol{u}_1) - \mu\nabla \times \nabla \times \boldsymbol{u}_1 - \rho\frac{\partial^2 \boldsymbol{u}_1}{\partial t^2} = = \alpha(3\lambda + 2\mu)\nabla T \tag{2}$$

where T is the temperature rise in the metal, k is the thermal conduction coefficient, ρ is the density, C_v is the constant volume specific heat, $Q(r, z, t)$ is the power density of the heat source created by laser irradiation expressed in two-

dimensional cylindrical coordinates (r, z), α is the linear thermal expansion coefficient, λ and μ are the Lamé constants and $\boldsymbol{u_1}$ is the displacement vector due to the thermoelastic effect. If we assume that no heat is lost from the target into air by conduction or radiation and that the entering pulsed laser is entirely absorbed at the surface, the source term in the heat conduction Eq. (1) becomes:

$$Q(r,z,t) = Q_o f(r) g(t) \delta(z) \qquad (3)$$

Q_o is the total absorbed heat, *f(r)* is the radial distribution of the laser irradiance, *g(t)* gives its temporal distribution whereas the term *δ(z)* considers the effect of absorption.
The elastic wave equation is then obtained from Newton's second law:

$$\rho \frac{\partial^2 \boldsymbol{u_2}}{\partial t^2} - \nabla \boldsymbol{s} = \boldsymbol{F_v} \qquad (4)$$

where $\boldsymbol{u_2}$ is the displacement vector due to the elastic effect, $\boldsymbol{s}$ is the stress tensor and $\boldsymbol{F_v}$ represents the volume force vector.

3. Use of COMSOL Multiphysics

A 2D axisymmetric model has been performed simulating the half cross section of an aluminium disk of radius 10 mm and 3 mm thick.

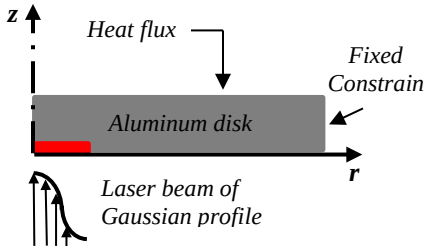

Figure 2. Schematic view of numerical model.

Two different physics have to be considered in Laser-Ultrasonics: thermo-elasticity for the ultrasonic wave generation due to the thermo-stress induced by the laser impulse and acoustics for the ultrasonic wave propagation within the material. The initial values for temperature and displacement field at t=0 are:

- T_0 = 293.15 K;
- **u**(0) = (0,0) in *r* and *z* directions.

The heat flux on the top surface simulates convective cooling. Except the top surface, all other boundaries are assumed to be thermally insulated.
The body heat load within the aluminum disk is given by the following expression:

$$Q_{in}(r,z,t) = Q(t)(1-R_c)\left(\frac{A_c}{\pi\sigma_r^2}\right) e^{-\left(\frac{r^2}{2\sigma_r^2}\right)} e^{-A_c z} \qquad (5)$$

where σ_R is the standard deviation of the Gaussian laser beam ($w_0/2$, being w_0 the laser beam waist size). The value assumed by σ_R in the model is 0.15 mm. The Aluminum thermal, mechanical and optical properties which appear in the equations (1), (2) and (5) have been reported in Table 1.

Table 1: Aluminum mechanical/thermal/optical properties

ρ	Density	2700 kg/m^3
C_p	Heat capacity at constant pressure	900 J/(kg K)
k	Thermal conductivity	160 W/(m K)
α	Coefficient of thermal expansion	23e-6 K^{-1}
R_C	Reflection coefficient	0.9

The time-dependence of the power thermal density *Q(t)* irradiated by the laser pulse is taken into account in the equation (5) using a triangular function with 12 ns of duration. The peak of the power emitted is 14 MW (Q_o).

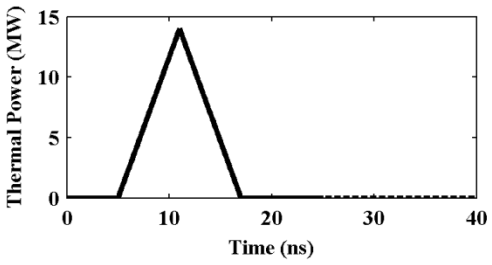

Figure 3. Triangle pulse simulating the time dependence of the power thermal density *Q(t)*.

In order to investigate the effect of thermoelastic expansion in terms of ultrasound waves propagation, the solid-acoustic interaction module has been added. The acoustic model

allows to connect the elastic wave propagation with the thermal deformation evaluated in the thermal stress module. Prescribed displacement (in r and z directions) boundary condition has been set in order to impose the thermal displacement, output of the thermal stress module, as input of the acoustic one.
A structured quadrilateral mesh with maximum dimension size of 1 μm was used. Distribution node configuration has been used in order to increase the number of element in the heat source region.
The simulation time has been 5 μs, which is enough for detecting all phenomena implied in the process.
The solver used is the time dependent-solver, with the generalized alpha method for computing the time step.

4. Experimental set-up for model validation

The model has been calibrated and validated through an experimental test performed on aluminum sample realized on purpose.

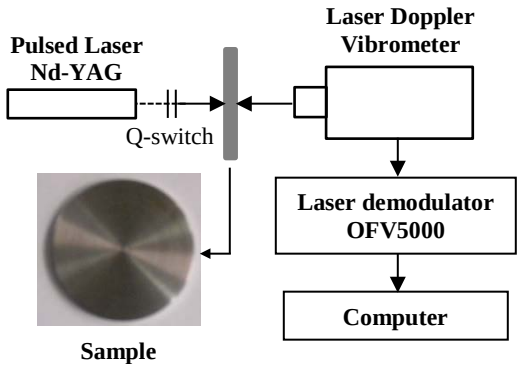

Figure 4. Experimental set-up.

The ultrasonic waves have been generated by a pulsed Nd-Yag laser emitting in the IR range and the surface displacement produced by the wave propagation measured by a Laser Doppler Vibrometer with a frequency bandwidth of 20 MHz, allowing a high spatial resolution (less than 1 mm).

5. Results

The test sample realized in the model is shown in Figure 5 where the different bulk waves propagation is visible.
The comparison with the experimental results has been done along a scanning line (red dots in Figure 5a).
It should be noticed that in the experimental tests, where a focused laser beam of 0.6 mm diameter and a power Q_o of 14 MW was used, the ultrasounds were generated in a slight ablation regime. On the other hand the numerical model took into account only the thermoelastic regime, neglecting the momentum transfer in the aluminium disc due to material ejection produced by laser ablation phenomenon.

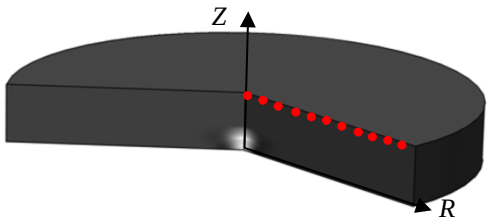

(a) Longitudinal (P) wave starting (t=0.2 μs).

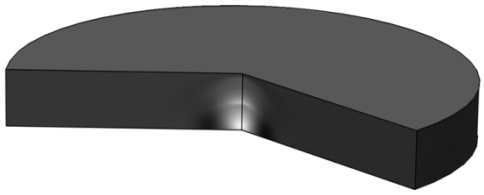

(b) P wave arrival at the epicentric face (t=0.4 μs) together with the arrival of the transverse wave (T) at about half thickness.

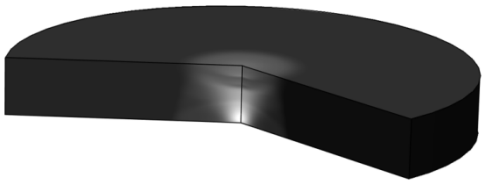

(c) Surface wave propagation through the epicentric face (t=1 μs).

Figure 5. 3D visualization of the elastic waves propagation.

Figure 6 shows the arrival times of the compressional (P) and shear (S) waves in the epicentric point obtained from numerical simulation using a laser beam of 0.6 mm diameter (σ_R = 0.15 mm).

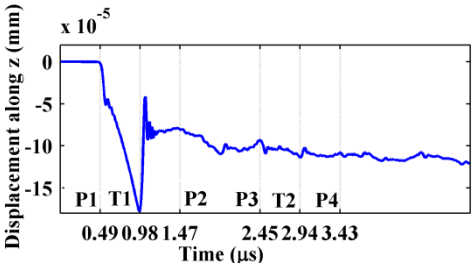

Figure 6. Displacement in the z-direction at the epicentric position.

The longitudinal wave propagates faster than the shear wave i.e. it arrives at the specimen plane after 0.49 μs (P1) propagating at the speed of 6123 m/s. The thermoelastic effect generates a dilation along the radial direction and a contraction of the material in the *z* direction creating a negative displacement at the epicentric position.

The shear wave arrives at 0.98 μs (T1) which propagates with roughly half the speed of the P-wave**.**

In Figure 6 the arrival times of reflected longitudinal waves in the *z* direction up to the 4th order (from P2 to P4) and the transverse wave second order (T2) are evident.

Figure 7 and 8 shows the numerical and experimental B-scans respectively, i.e. the waterfall plot of the surface displacement in *z*-direction with respect to time (in abscissa) and spatial position along the scanning line, reported in Figure 5a (in ordinate), in the following conditions:

- laser diameter (σ_R) of 0.6 mm,
- laser energy of 140 mJ and,
- laser pulse duration of 12 ns.

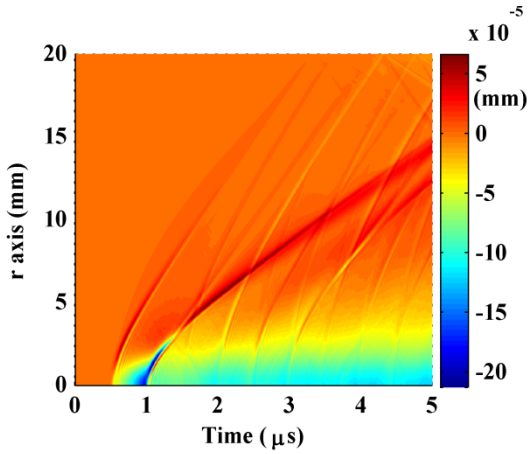

Figure 7. Waterfall of the numerical displacement in the *z*-direction.

The waterfalls represent the displacement in the *z*-direction on the epicentric surface (the position at 0 mm corresponds to the epicentric position).

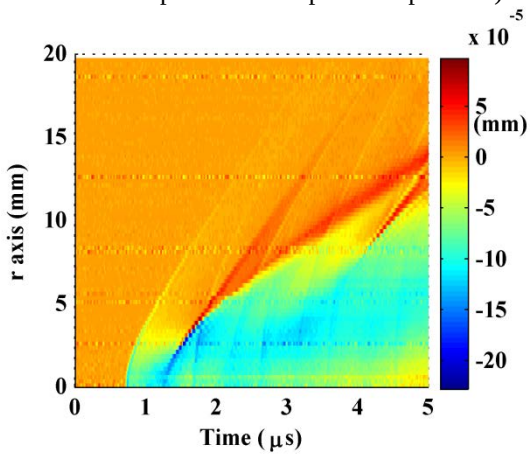

Figure 8. Waterfall of the experimental displacement in the *z*-direction.

Figure 9 shows typical dispersion curves in the normalized wavenumber(k)-frequency(ω) domain ($\omega h/c_S$, kh) for Lamb waves together with the curves for the longitudinal and shear waves. The normalization has been performed taking into account the test object thickness (h) and the shear bulk wave speed (c_S). The dispersion curves have been obtained with a simulation time of 100 μs. The spatial/frequency resolution of the analysis is not sufficient to separate the different Lamb waves components, but their distribution is clearly visible.

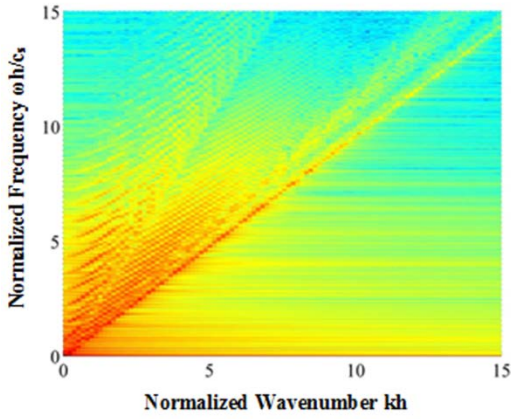

Figure 9. Theoretical dispersion curves of Rayleigh-Lamb frequency equations.

As mentioned in the beginning of this section the numerical model does not consider ablation phenomena which occur when the laser beam exceed a certain energy density. In the case of focused laser beam ablation always arise even though it has been demonstrated that the numerical model results accurately follows the experimental ones, see B-scans in Figures 7 and 8. However the displacement amplitude calculated at the epicentric position is lower than the one measured in the experiments because of the ablation effect. Therefore the quantitative comparison between displacement amplitude calculated numerically and measured experimentally has been done repeating the experiment with a collimated laser beam (laser diameter of 6 mm). The same laser waist (σ_R = 6 mm) has been set in the numerical model.

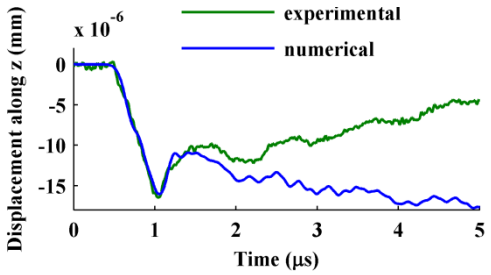

Figure 10. Displacement in the *z*-direction at the epicentric position obtained from numerical simulation (blue line) and experimental test (green line).

Figure 10 shows a comparison between experimental and numerical models for the displacement values in the *z*-direction at the epicentric position. Apart from a small positive initial pulse (due to the thermal diffusivity), both displacement waveforms are negative, confirming that the surface at the epicentric position is compressed.
The arrival times of the P-waves are the same in both the experimental and numerical analysis (about 0.49 μs).

7. Conclusions

The paper illustrated the results obtained with a multi-physics numerical model for the complete characterization of the physical mechanism governing the emission and the interaction of the ultrasonic wave with metallic materials in laser ultrasonics. The model has been validated with experimental data, showing a good correspondence both in terms of propagation mechanisms (P, T bulk waves) and ultrasonic wave amplitude.
In a future work the model will be exploited to perform a sensitivity analysis to the laser characteristic parameters (i.e. laser energy, diameter and pulse duration). Once validated the model, these parameters can be set in advance in relation to the measurement conditions, testing object material and damage typologies (i.e. surface or in-depth defect, convex defect due to fatigue or concave defect due to fretting, defect dimension).
The research is funded by Ministry of Instruction, Research and Education in a PRIN project.

8. References

1. C.B. Scruby, L.E. Drain, *Laser Ultrasonics Techniques and Applications*, Ed. Taylor & Francis Group, (1990).
2. T. Stratoudaki, C. Edwards, S. Dixon, S.B. Palmer, Advances In Laser Based Ultrasound In Carbon Fibre Reinforced Composites For Aircraft Inspection, *NDT.net* 8 (2), (2003).
3. C. Edwards, T. Stratoudaki, S. Dixon, S. Palmer, Laser generated ultrasound: efficiency and damage thresholds in carbon fibre reinforced composites, *IEE Proceedings - Science, Measurement and Technology*, 148 (4), 139-142 (2001).

4. M. Dubois, F. Enguehard, L. Bertrand, Modeling of laser thermoelastic generation of ultrasound in an orthotropic medium, *Applied Physics Letters*, (64) (5), 554-556 (1994).
5. C.B. Scruby, R. J. Dewhurst, D.A. Hutchins, S.B. Palmer, Quantitative studies of thermally generated elastic waves in laser-irradiated metals, *Journal of Applied Physics*, 51 (12), 6210-6216 (1980).
6. R.J. Dewhurst, C. Edwards, A. D. W. McKie, S.B. Palmer, Estimation of the thickness of thin metal sheet using laser generated ultrasound Appied. Physics Letter, 51 (14), 1066-1068 (1987).
7. P.A. Doyle, On epicentral waveforms for laser-generated ultrasound, *Journal of Physics D: Applied Physics*, 19, 1613-1623 (1986).
8. F. Alan McDonald, On the precursor in laser-generated ultrasound waveforms in metals Applied Physics Letters, 56 (3), 230-232 (1990).
9. P. Castellini, G.M. Revel, L. Scalise, R.M. De Andrade, Experimental and numerical investigation on structural effects of laser pulses for modal parameter measurement, *Optics and Lasers in Engineering*, 32, 565-581 (2000).
10. P. Zhang, C.F. Ying, J. Shen, Directivity patterns of laser thermoelastically generated ultrasound in metal with consideration of termal conductivity, *Ultrasonics*, 35, 233-240 (1997).